Rapid Communications

Quantum oscillations and a nontrivial Berry phase in the noncentrosymmetric topological superconductor candidate BiPd

Mojammel A. Khan,[1,*] D. E. Graf,[2] I. Vekhter,[1] D. A. Browne,[1] J. F. DiTusa,[1] W. Adam Phelan,[1,†] and D. P. Young[1]

[1]*Department of Physics and Astronomy, Louisiana State University, Baton Rouge, Louisiana 70803, USA*

[2]*National High Magnetic Field Laboratory, Tallahassee, Florida 32310, USA*

(Received 23 January 2018; revised manuscript received 16 January 2019; published 29 January 2019)

We report the measurements of de Haas-van Alphen (dHvA) oscillations in the noncentrosymmetric superconductor BiPd. Several pieces of a complex multisheet Fermi surface are identified, including a small pocket ($\alpha \sim 40$ T) which is three dimensional and anisotropic. From the temperature dependence of the amplitude of the oscillations, the cyclotron effective mass is $(0.18 \pm 0.02)\, m_e$. Further analysis revealed a nontrivial π-Berry phase is associated with the 40 T pocket, which strongly supports the presence of topological states in bulk BiPd.

DOI: 10.1103/PhysRevB.99.020507

Topological materials, such as topological insulators (TI) and superconductors (TSC's), are of great current interest because their complex electronic structure underlies properties that hold promise for practical applications, such as spintronics and quantum computation [1–7]. The essential ingredient is the spin orbit coupling (SOC) that creates nontrivial band states [1,3]. In a TSC, it is the wave function of the electron pairs that exhibits topological properties, and among the most promising candidates for topological superconductivity are materials with noncentrosymmetric (NCS) crystal structures. In NCS superconductors, the lack of an inversion center in the crystal lattice may lead to strong antisymmetric SOC and hence to a complex order parameter with mixed spin singlet and spin triplet pairing components [8–10]. This can result in topologically nontrivial superconducting phases, characterized by a full superconducting gap in the bulk, but supporting a protected zero-energy mode at the vortex core (Majorana fermion), as well as gapless edge or surface states [11–13]. These latter states are a consequence of Andreev reflection at the boundaries and hence are referred to as Andreev bound states (ABS) [14]. Thus, the NCS family of superconductors is most auspicious for hosting topological superconductivity [15–19]. Thus far, few topological NCS superconductors have been identified [20–22], but the effort to identify new such materials continues.

The NCS chiral lattice compound BiPd is a type-II superconductor with a transition temperature of $T_c \sim 3.8$ K [23,24], which has attracted much interest recently due to the possible unconventional nature of its superconductivity. Here, the unconventional superconducting state is thought to be due to the large SOC caused by the presence of the heavy element Bi [25]. Surface experiments performed on BiPd thus far show Dirac surface states [24,25] with anisotropic behavior [26], albeit these states are far from the chemical potential. A scanning tunneling microscopy (STM) study found a strong zero bias conductance peak (ZBCP) in the vortex core [25]. The ZBCP was attributed to the vortex core state, but the experiment lacked the resolution to determine whether these were Majorana modes and therefore could not definitively determine whether the system is topological [25,27]. Importantly, directional point contact Andreev reflection (PCAR) measurements also observed a ZBCP, along with evidence for multiple superconducting gaps [28], suggesting an unconventional order parameter. Andreev surface states emerge for certain surface orientations in topologically trivial nodal superconductors, but such an explanation appears to be at odds with thermal and charge transport measurements which indicate an isotropic, fully gapped, superconducting state in the bulk [29,30]. In fact, many of the properties observed in BiPd are similar to those of other TSC candidates, such as $Cu_{0.25}Bi_2Se_3$ [7] and $PbTaSe_2$ [20]. For example, $Cu_xBi_2Se_3$ displays a similar ZBCP in PCAR measurements that was attributed to the existence of Majorana fermions and hence topological superconductivity [14]. Clearly, further investigations to probe the topological nature of BiPd are needed.

The difficulty in providing direct evidence for topology is that few probes directly couple to the phase of the wave function. Recently, quantum oscillations under applied magnetic fields were used to determine the topological nature of the bands in a number of compounds [31–35] through measurements of a nontrivial π-Berry phase of electronic carriers. To our knowledge no such data have been reported for BiPd, and in this paper, we report quantum oscillations in single crystalline BiPd measured by torque magnetometry, i.e., the de Haas-van Alphen (dHvA) effect, for different orientations of the magnetic field (H). Analysis of the dHvA data suggests a complex three-dimensional Fermi surface composed of multiple sheets. We focus on a pocket with the dHvA frequency of 40 T, since we can track the signal over a wide range of fields and temperatures. We find that these charge carriers have a very small mass $(0.18 \pm 0.02)m_e$, where m_e is the bare electron mass. We show that a nontrivial Berry phase exists for the same frequency oscillation, indicating Dirac-like properties with nontrivial topology.

*mkhan19@lsu.edu, mkhan19@anl.gov

†Current address: Department of Chemistry, The Johns Hopkins University, Bloomberg 105, Baltimore, MD 21218, USA

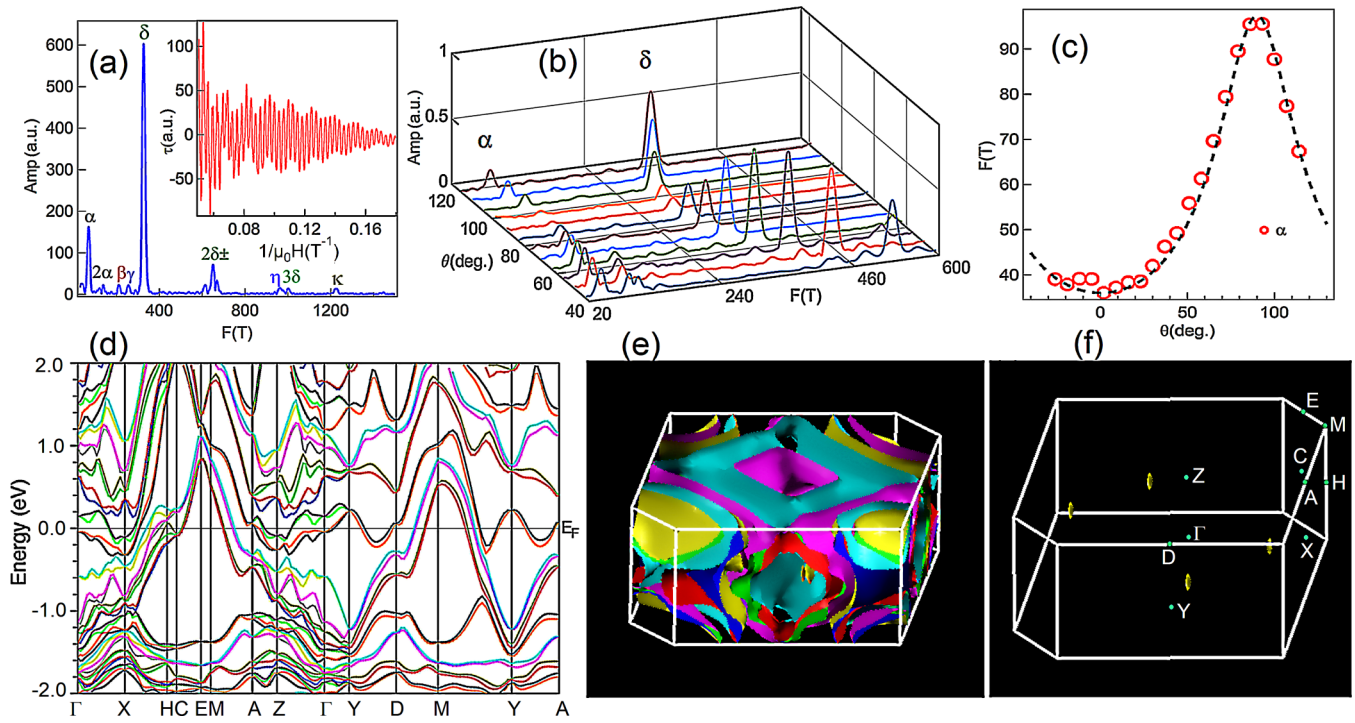

FIG. 1. Quantum oscillations detected via torque response, τ, in arbitrary units (a.u.), of the cantilever magnetometer at 0.35 K. (a) Fast Fourier transform (FFT) of the data shown in the inset for the field range from 5 to 20 T. The primary frequencies α, β, γ, δ, η, and κ, and higher harmonics, are labeled. Inset: Torque response of the cantilever magnetometer at 0.35 K with field applied 70° from the b axis showing dHvA oscillations in inverse field, $1/\mu_0 H$. (b) Frequency change with orientation of the magnetic field as the sample is rotated between 42° and 119° with θ representing the angle between the field and the b axis. A complete list of fundamental frequencies and their dispersion is given in the Supplemental Material [36]. (c) Angular dependence of α. The frequency can be well described by a 3D anisotropic ellipsoid (dashed line), which corresponds to a 3D piece of Fermi surface with ellipticity of 2.7. (d) GGA+spin orbit coupling (SOC) band structure of BiPd. (e) GGA+SOC Fermi surface of BiPd projected into the first Brillouin zone. Several electron and hole pockets can be identified in the zone center as well as around the corners. (f) The α frequency projected in the Brillouin zone is anisotropic conical ellipsoid, in agreement with the experimental data. The calculated mass is 0.14 m_e, which is similar to that found from dHvA measurements.

Single crystals of BiPd were synthesized using a modified Bridgman technique in a radio-frequency induction furnace. Large crystals were produced that were easily cleaved. A cleaved piece was analyzed using x-ray diffraction (XRD) which showed reflections from the (0 k 0) plane only (Supplemental Materials (SM) [36], Fig. S1), indicating the cleaved surface is perpendicular to the unique axis (b axis) of its monoclinic structure. A standard four-probe resistivity measurement showed a superconducting transition $T_c \sim 3.8$ K with a residual resistivity ratio (RRR, $\rho_{290\,\mathrm{K}}/\rho_{4\,\mathrm{K}}$) greater than 100, indicating excellent crystal quality (see SM [36], Fig. S2). The measurement of quantum oscillations was performed at the NHMFL in Tallahassee, FL employing a torque magnetometry technique using the 35 T resistive magnet in a cryostat with a base temperature of 350 mK. A complete XRD analysis and details of the measurement techniques are discussed in the SM [36].

Clear periodic oscillations were observed in the torque measurements, as shown in Fig. 1(a), with the magnetic field applied 70° from the b axis at 0.35 K. At this angular position, the oscillations contain a maximum number of frequencies which were extracted by fast Fourier transformation (FFT). Among those, the 40 T frequency (α) is present over the entire angular range [Figs. 1(b), 1(c), and S3]. Several other frequencies appear at different field directions and then disappear, as the direction of the applied field is varied with respect to the crystallographic b axis. The existence of multiple frequencies in the dHvA oscillations are consistent with a complex multisheet Fermi surface, evident from the calculated electronic structure [Fig. 1(d)] and Fermi surface projected in the first Brillouin zone which can be seen in Figs. 1(e) and 1(f). Our calculated electronic structure is similar to previously published work [26]. The details of the electronic structure calculations are given in the SM [36].

Rotating the sample with respect to the applied field reveals the angular dependence of the dHvA frequencies [Fig. 1(b)]. We observed a moderate change with angle (θ), in the small frequency α. The value of this frequency increases to a maximum at $\theta \sim 90°$, i.e., field along the ac plane. The angular dependence of α can be fitted with a form appropriate for a three-dimensional ellipsoid, where the ellipticity was found to be ~2.7, as seen in Fig. 1(c). Thus, α is an anisotropic, three-dimensional (3D) pocket of Fermi surface. The smallest extremal cross-sectional area, S_F, of the frequency α can be estimated by the Onsager formula (see SM [36]) and was found to be $S_F = 3.81\times10^{-3}$ Å^{-2}. This corresponds to about 0.5% of the total Brillouin zone area in the $k_x - k_z$ (ac) plane. All the fundamental frequencies extracted from the dHvA oscillations and their corresponding S_F values are listed in Table S1 of the SM [36]. Figure 1(f) shows the location of the

Fermi surface sheet consistent with the measured properties of the α frequency in the first Brillouin zone. This sheet lies close to the Γ-X and Γ-Y lines but far enough away from these high symmetry directions such that the crossing of this band through the Fermi energy is not readily apparent in Fig. 1(d). However, careful inspection of the bands in this region of the Brillouin zone revealed that, within the precision of the calculation, the dispersion of this band is anisotropic and conical (Dirac-like) and that the conical structure is only found if SOC is included. This suggests that the α band may have topological character, and we investigate it further below.

We analyze the dHvA oscillations by fitting the oscillatory magnetization to the Lifshitz-Kosevich (LK) formula [32,40,41],

$$\Delta M \propto -B^{\lambda} R_T R_D R_S \, sin\left[2\pi\left(\frac{F}{B} - \gamma_p - \delta_p\right)\right]. \quad (1)$$

Here, R_T is the thermal damping term, which defines the effective mass of the band carriers, and R_D is the Dingle damping factor [41]. Both of these factors are due to Landau level (LL) broadening, which is caused by the effects of finite temperature, R_T, and carrier scattering rates, R_D. The term R_S is the spin reduction factor, which is related to the Zeeman effect. A more in depth description of each of these terms is given in the SM [36]. Finally, the oscillation is described by a sinusoidal term that contains the phase factor $(-\gamma_p - \delta_p)$, where γ_p is related to the Berry phase Φ_B as $\gamma_p = \frac{1}{2} - \frac{\Phi_B}{2\pi}$. The dimension of the Fermi pocket characterizes the value of λ and δ_p. For example, for a 3D Fermi surface, the values are 1/2 and $\pm 1/8$ (+ for minimal and − for a maximal cross section of the constant energy surface), respectively [32].

The temperature dependence of the amplitude of the oscillations was investigated with the field applied at an angle of 28° with respect to the b axis and can be seen in Fig. 2(a). At this angular position, only the α frequency dominates and persists at temperatures as high as 20 K. This indicates a light mass for the band carriers associated with this frequency. By using the data up to 15 K, we determined the effective mass for this mode as $m^* = (0.18 \pm 0.02)m_e$ from a fit to the form for R_T described in the SM [36], where m_e is the bare electron mass [Fig. 2(b)]. The amplitudes of the other frequencies drop abruptly with increased temperature as can be seen in Fig. 2(a) and the inset of Fig. 2(b), preventing an accurate estimation of the effective mass associated with the other oscillatory modes. For example, using only a limited number of data points (three for the frequency mode β), the effective mass of the frequency was estimated to be $(0.55 \pm 0.05)\mathrm{m}_e$ (see Fig. S5 in the SM [36]).

Figure 3(a) displays the results of a fit of the LK theory, Eq. (1), to the oscillation amplitude at 10 K with magnetic field applied at 28° with respect to the b axis. We choose to analyze the data at this particular temperature since the higher frequencies were substantially damped, so that the oscillations associated with the 40 T frequency were clearly dominant. The best fit of this form to the data results in a frequency of 41.0 ± 0.2 T, which matches the frequency found in the FFT analysis. In addition, we determine a phase factor, $(-\gamma_p - \delta_p)$, in Eq. (1), that is small, -0.06 ± 0.01, indicating a nontrivial

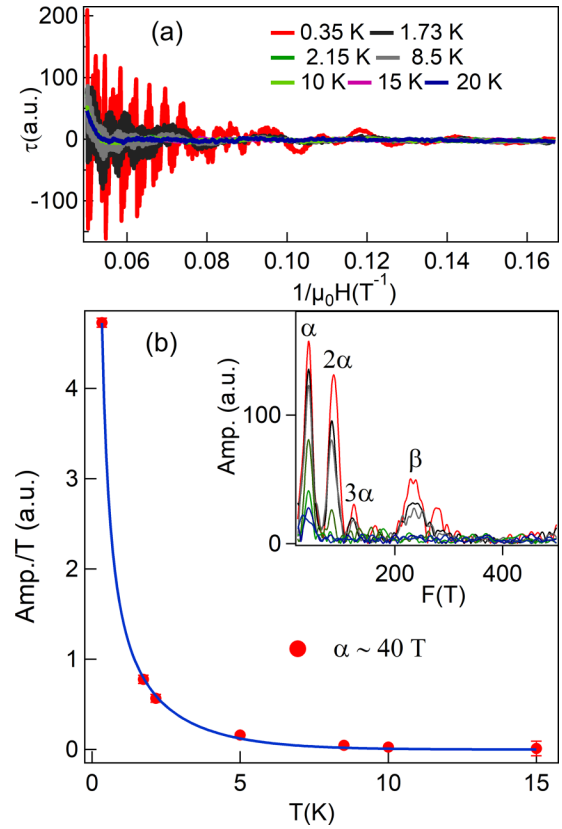

FIG. 2. Effective mass of the band carriers. (a) Temperature dependence of the de Haas-van Alphen oscillation amplitude, τ, in the field range from 5 to 20 T. (b) Temperature, T, dependence of the normalized oscillation amplitude (amplitude/T, red circles), along with a fit (solid line) of the LK theory (R_T) as described in the text. Inset: FFT of the oscillations shown in (a).

Berry phase. If we assume the minimal cross section ($\delta_p = \frac{1}{8}$), we find $\Phi_B = (1.13 \pm 0.01)\pi$, while for a maximal cross section ($\delta_p = -\frac{1}{8}$), we find $\Phi_B = (0.63 \pm 0.01)\pi$. This result strongly suggests a nontrivial topological nature of the α band.

The value of the Berry phase can also be extracted from a Landau level (LL) fan diagram, since the density of states is proportional to dM/dB [31,41,42]. To further investigate the frequency α, we isolated [inset of Fig. 3(b)] and indexed the oscillation minima as $(n - 1/4)$ [31,42] and maxima as $(n + 1/4)$ and plotted them versus the corresponding inverse field value. The Berry phase can then be estimated using the intercept n_0, i.e., $\Phi_B = 2\pi(n_0 + \delta_p)$, where δ_p is defined as above. From the fit to the filtered data [Fig. 3(b)], the intercept n_0 is 0.46 ± 0.05. Using this value, the Berry phase is $(1.17 \pm 0.05)\pi$ for the minimal cross section or $(0.67 \pm 0.05)\pi$ for the maximal cross section. These values are consistent with the phase determined from the LK fit. Furthermore, the slope of the line in Fig. 3(b) is 40.9 ± 0.6 T, which is within our measurement uncertainty of the frequency determined from the FFT analysis and the LK fit.

The Dingle temperature T_D can be estimated from the magnetic field dependence of the dHvA amplitude through a comparison to Eq. (1), where the term R_D contains this dependence (see SM [36]). From a fit of this form to the field dependence of the α frequency (Fig. S5b), we find $T_D = 8 \pm 2$ K.

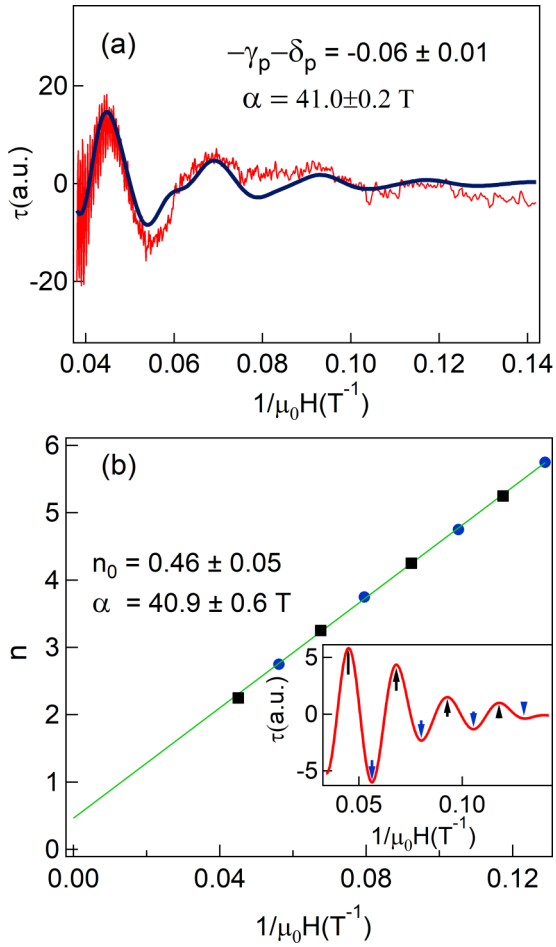

FIG. 3. Berry phase analysis. (a) de Haas-van Alphen data at 10 K (red line) vs inverse field, $1/\mu_0 H$. Solid blue line is a fit of the LK theory to the data. Two higher harmonics and the principal frequency were used in the fit to the data over a broad field range from 7 to 26 T. (b) LL-fan diagram. Blue circles represent minima of the oscillations as demonstrated by the arrows in the inset, while black squares represent the maxima. The solid line is a linear fit. Inset: Data after applying a bandpass filter to the torque data around the 40 T frequency. Arrows indicate the positions of the maxima (black) and minima (blue).

From T_D the relaxation time, τ_q, and subsequently the mobility, μ_q, can be estimated through the relations $\tau_q = \frac{\hbar}{2\pi K_B T_D}$, and $\mu_q = \frac{e\tau_q}{m^*}$ [41]. Our data are thus consistent with $\tau_q = 1.5\times10^{-13}$ s and a large mobility $\mu_q = 1465$ cm^2/Vs. Large mobility is typical of topologically nontrivial states and is found in almost all topological compounds such as TIs and Dirac materials [4,6]. Thus, our analysis indicates that the α frequency corresponds to a topologically nontrivial band with a small effective mass and high mobility. 3D Dirac systems lacking inversion symmetry generally support nontrivial topological states over a wide range of parameters of the Hamiltonian (in contrast to inversion-symmetric counterparts) [43,44]. In this case, observation of the nontrivial Berry phase shown in Fig. 3, combined with the dispersion of the α band, which is, within the precision of the calculations, linear and consistent with a tilted cone close to the Fermi surface, strongly supports placing BiPd in the topologically-nontrivial regime, consistent with Ref. [26]. Moreover, this quasiconical structure appears only when SOC is included.

The nontrivial topology of the α band infers topological superconductivity in that band [45,46]. While this band alone may not be driving the superconductivity in BiPd, it is well known, see, e.g., Ref. [47], that quasiparticle interactions induce superconductivity on all Fermi surface sheets. Even when the induced order parameter is small on some sheets, the effect is algebraic, rather than exponential, in the quasiparticle interaction. Therefore, in the absence of any potential pair-breaking due to disorder, i.e., in clean samples, our findings point to a nontrivial superconducting order parameter at one of the sheets of the Fermi surface of BiPd.

In summary, we have measured dHvA oscillations in high-quality single crystals of the NCS superconductor BiPd. FFT analysis revealed multiple frequencies associated with a complex Fermi surface. Among those, we focused on the lowest frequency oscillation, α, which corresponds to a small pocket of the Fermi surface that we determined to be three-dimensional and anisotropic. Crucially, the analysis of the phase of the oscillations revealed a nontrivial Berry phase associated with the carriers in this pocket. Our work shows evidence for the topological nature of the bulk carriers in BiPd and provides motivation to further study the nature of the bulk multiband superconductivity and detailed conditions for the existence of any topological superconducting states.

D.P.Y. acknowledges support from the NSF under Grant No. DMR-1306392 for materials synthesis, conductivity, and dHvA measurements. J.F.D. and D.P.Y. were supported by the U.S. Department of Energy under EPSCoR Grant No. DE-SC0012432 with additional support from the Louisiana Board of Regents for XRD measurements and data analysis. I.V. acknowledges support from NSF Grant No. DMR-1410741 for theoretical analysis. Portions of this work were performed at the NHMFL, which is supported by NSF Cooperative Agreement No. DMR-1157490 and the State of Florida, and the Analytical Instrumentation Facility (AIF) at North Carolina State University, supported by the State of North Carolina and the NSF award number ECCS-1542015. We acknowledge Dr. C. Loehn at Shared Instrumentation Facility (SIF), LSU for chemical analysis and Dr. C.-C. Chung (AIF) for the temperature dependent x-ray diffraction measurements.

[1] L. Fu, C. L. Kane, and E. J. Mele, Phys. Rev. Lett. **98**, 106803 (2007).

[2] Y. L. Chen, J. G. Analytis, J.-H. Chu, Z. K. Liu, S.-K. Mo, X. L. Qi, H. J. Zhang, D. H. Lu, X. Dai, Z. Fang, S. C. Zhang, I. R. Fisher, Z. Hussain, and Z.-X. Shen, Science **325**, 178 (2009).

[3] Y. Xia, D. Qian, D. Hsieh, L. Wray, A. Pal, H. Lin, A. Bansil, D. Grauer, Y. S. Hor, R. J. Cava, and M. Z. Hasan, Nat. Phys. **5**, 398 (2009).

[4] M. Z. Hasan and C. L. Kane, Rev. Mod. Phys. **82**, 3045 (2010).

[5] M. König, S. Wiedmann, C. Brüne, A. Roth, H. Buhmann, L. W. Molenkamp, X.-L. Qi, and S.-C. Zhang, Science **318**, 766 (2007).

[6] X.-L. Qi and S.-C. Zhang, Rev. Mod. Phys. **83**, 1057 (2011).

[7] Y. S. Hor, A. J. Williams, J. G. Checkelsky, P. Roushan, J. Seo, Q. Xu, H. W. Zandbergen, A. Yazdani, N. P. Ong, and R. J. Cava, Phys. Rev. Lett. **104**, 057001 (2010).

[8] E. Bauer and M. Sigristz, *Non-centrosymmetric Superconductors: Introduction and Overview* (Springer-Verlag, Heidelberg, 2012).

[9] M. A. Khan, A. B. Karki, T. Samanta, D. Browne, S. Stadler, I. Vekhter, A. Pandey, P. W. Adams, D. P. Young, S. Teknowijoyo, K. Cho, R. Prozorov, and D. E. Graf, Phys. Rev. B **94**, 144515 (2016).

[10] F. Kneidinger, E. Bauer, I. Zeiringer, P. Rogl, C. Blaas-Schenner, D. Reith, and R. Podloucky, Physica C **514**, 388 (2015).

[11] J. C. Y. Teo and C. L. Kane, Phys. Rev. Lett. **104**, 046401 (2010).

[12] X.-L. Qi, T. L. Hughes, S. Raghu, and S.-C. Zhang, Phys. Rev. Lett. **102**, 187001 (2009).

[13] S. Deng, L. Viola, and G. Ortiz, Phys. Rev. Lett. **108**, 036803 (2012).

[14] S. Sasaki, M. Kriener, K. Segawa, K. Yada, Y. Tanaka, M. Sato, and Y. Ando, Phys. Rev. Lett. **107**, 217001 (2011).

[15] M. Sato and S. Fujimoto, Phys. Rev. B **79**, 094504 (2009).

[16] A. P. Schnyder and S. Ryu, Phys. Rev. B **84**, 060504 (2011).

[17] K. Samokhin, Ann. Phys. **359**, 385 (2015).

[18] B. Béri, Phys. Rev. B **81**, 134515 (2010).

[19] A. Daido and Y. Yanase, Phys. Rev. B **95**, 134507 (2017).

[20] G. M. Pang, M. Smidman, L. X. Zhao, Y. F. Wang, Z. F. Weng, L. Q. Che, Y. Chen, X. Lu, G. F. Chen, and H. Q. Yuan, Phys. Rev. B **93**, 060506 (2016).

[21] S.-Y. Guan, P.-J. Chen, M.-W. Chu, R. Sankar, F. Chou, H.-T. Jeng, C.-S. Chang, and T.-M. Chuang, Sci. Adv. **2**, e1600894 (2016).

[22] Z. Liu, L. Yang, S.-C. Wu, C. Shekhar, J. Jiang, H. Yang, Y. Zhang, S.-K. Mo, Z. Hussain, B. Yan *et al.*, Nat. Commun. **7**, 12924 (2016).

[23] Y. Bhatt and K. Schubert, J. Less-Common Met. **70**, P39 (1980).

[24] H. M. Benia, E. Rampi, C. Trainer, C. M. Yim, A. Maldonado, D. C. Peets, A. Stöhr, U. Starke, K. Kern, A. Yaresko, G. Levy, A. Damascelli, C. R. Ast, A. P. Schnyder, and P. Wahl, Phys. Rev. B **94**, 121407 (2016).

[25] Z. Sun, M. Enayat, A. Maldonado, C. Lithgow, E. Yelland, D. C. Peets, A. Yaresko, A. P. Schnyder, and P. Wahl, Nat. Commun. **6**, 6633 (2015).

[26] S. Thirupathaiah, S. Ghosh, R. Jha, E. D. L. Rienks, K. Dolui, V. V. Ravi Kishore, B. Büchner, T. Das, V. P. S. Awana, D. D. Sarma, and J. Fink, Phys. Rev. Lett. **117**, 177001 (2016).

[27] C. Caroli, P. D. Gennes, and J. Matricon, Phys. Lett. **9**, 307 (1964).

[28] M. Mondal, B. Joshi, S. Kumar, A. Kamlapure, S. C. Ganguli, A. Thamizhavel, S. S. Mandal, S. Ramakrishnan, and P. Raychaudhuri, Phys. Rev. B **86**, 094520 (2012).

[29] X. B. Yan, Y. Xu, L. P. He, J. K. Dong, H. Cho, D. C. Peets, J.-G. Park, and S. Y. Li, Supercond. Sci. Technol. **29**, 065001 (2016).

[30] B. Joshi, A. Thamizhavel, and S. Ramakrishnan, Phys. Rev. B **84**, 064518 (2011).

[31] Y. Ando, J. Phys. Soc. Jpn. **82**, 102001 (2013).

[32] J. Hu, Z. Tang, J. Liu, X. Liu, Y. Zhu, D. Graf, K. Myhro, S. Tran, C. N. Lau, J. Wei, and Z. Mao, Phys. Rev. Lett. **117**, 016602 (2016).

[33] Z. Ren, A. A. Taskin, S. Sasaki, K. Segawa, and Y. Ando, Phys. Rev. B **82**, 241306 (2010).

[34] A. Pariari, P. Dutta, and P. Mandal, Phys. Rev. B **91**, 155139 (2015).

[35] P. Sergelius, J. Gooth, S. Bäßler, R. Zierold, C. Wiegand, A. Niemann, H. Reith, C. Shekhar, C. Felser, B. Yan *et al.*, Sci. Rep. **6**, 33859 (2016).

[36] See Supplemental Material at http://link.aps.org/supplemental/10.1103/PhysRevB.99.020507 for experimental detail, XRD analysis, review of LK theory, and detail of electronic structure calculation (which includes Refs. [37–39]).

[37] Y. Bhatt and K. Schubert, J. Less-Common Met. **64**, P17 (1979).

[38] P. Blaha, K.-H. Schwarz, G. Madsen, D. Kvasnicka, and J. Luitz, *WIEN2k, An Augmented Plane Wave Plus Local Orbitals Program for Calculating Crystal Properties* (TU, Wien, 2001).

[39] J. P. Perdew, K. Burke, and M. Ernzerhof, Phys. Rev. Lett. **77**, 3865 (1996).

[40] I. M. Lifshitz and A. M. Kosevich, Sov. Phys. JETP **2**, 636 (1956).

[41] D. Shoenberg, *Magnetic Oscillations in Metals* (Cambridge University Press, Cambridge, UK, 2009).

[42] J. Xiong, Y. Luo, Y. H. Khoo, S. Jia, R. J. Cava, and N. P. Ong, Phys. Rev. B **86**, 045314 (2012).

[43] N. P. Armitage, E. J. Mele, and A. Vishwanath, Rev. Mod. Phys. **90**, 015001 (2018).

[44] S. Murakami, New J. Phys. **9**, 356 (2007).

[45] Z. Wang, H. Weng, Q. Wu, X. Dai, and Z. Fang, Phys. Rev. B **88**, 125427 (2013).

[46] X.-L. Qi, T. L. Hughes, and S.-C. Zhang, Phys. Rev. B **81**, 134508 (2010).

[47] V. Barzykin and L. P. Gor'kov, Phys. Rev. B **76**, 014509 (2007).